In situ detection with interdigitated array electrodes towards the platinum-catalyzed oxygen reduction reaction: size effect and the reaction pathway

Peiqi Du , Jinwen Shi , Jing Zhan , Lei Fu , Fei Liu

PII: S0040-6090(23)00419-4
DOI: https://doi.org/10.1016/j.tsf.2023.140089
Reference: TSF 140089

To appear in: *Thin Solid Films*

Received date: 2 May 2023
Revised date: 11 October 2023
Accepted date: 11 October 2023

Please cite this article as: Peiqi Du , Jinwen Shi , Jing Zhan , Lei Fu , Fei Liu , In situ detection with interdigitated array electrodes towards the platinum-catalyzed oxygen reduction reaction: size effect and the reaction pathway, *Thin Solid Films* (2023), doi: https://doi.org/10.1016/j.tsf.2023.140089

Highlights

- Direct synthesis of Pt was applied to avoid changing of surface status of Pt.
- Interdigitated array electrode was used for the *in-situ* detection of H_2O_2.
- The specific activity and mass activity are larger for the smaller-sized Pt.
- The proportion of different catalytic pathways can be calculated.
- The smaller-sized Pt undergoes about 43% of the 4-electron-pathway reaction.

In situ detection with interdigitated array electrodes towards the platinum-catalyzed oxygen reduction reaction: size effect and the reaction pathway

Peiqi Du[1], Jinwen Shi[*,2], Jing Zhan[1], Lei Fu[1], Fei Liu[*,1]

[1]School of Advanced Materials and Nanotechnology, Interdisciplinary Research Center of Smart Sensing, Xidian University, 266 Xinglong Section of Xifeng Road, Xi'an, Shaanxi, 710126, People's Republic of China

[2]International Research Center for Renewable Energy, State Key Laboratory of Multiphase Flow in Power Engineering, Xi'an Jiaotong University, 28 West Xianning Road, Xi'an, Shaanxi 710049, China.

[*]Correspondence: Fei Liu, fliu@xidian.edu.cn, Jinwen Shi, jinwen_shi@mail.xjtu.edu.cn

Abstract

Platinum has long been recognized as a vital catalyst in energy conversion and utilization, particularly in oxygen reduction reaction (ORR), due to its exceptional catalytic activity. However, its exorbitant cost and scarcity have motivated researchers to explore the size-activity correlation of Pt catalysts in ORR, aiming to reduce Pt loading density while preserving high catalytic performance. In this work, we concentrate on the interdigitated-array(IDA)-electrodes-based precise detection of the influence of Pt cluster size on catalytic ability, focusing on (1) Direct synthesis of Pt catalyst onto electrodes surface, rather than offline preparation and pasting, to avoid interference from other chemicals and changes to the surface status of catalyst particles; (2) Use of IDA electrodes with largely improved sensitivity for *in-situ* detection of reaction intermediates (H_2O_2) and provide insight into the reaction pathway and electron transfer process. It indicates that the specific activity and mass activity are larger for the smaller-sized Pt cluster. Specifically, the proportion of different electron transfer pathways was analyzed with IDA results, and with the same amount of Pt catalyst loading, the smaller-sized Pt cluster produces a higher percent of H_2O_2; the smaller-sized Pt catalyzed ORR undergoes less proportion of 4-electron pathway than the larger-sized Pt catalyst (about 43% total catalytic current is contributed by the 4-electron pathway for the #6 Pt catalyst, and this number raises to 98% for the #1 Pt catalyst).

Keywords: Platinum; Electrodeposition; Oxygen reduction reaction; Interdigitated array electrode; Sensor; Reaction intermediate; Peroxide

1. Introduction

Oxygen reduction reaction (ORR) is one of the essential fundamental reactions of energy storage and utilization and its sluggish reaction rate necessitates the development of highly efficient catalysts. Although platinum (Pt) and Pt-based catalysts exhibit high catalytic activity, their high cost and limited availability continue to be a concern. Therefore, improving the electrocatalytic activity of Pt-based catalysts while minimizing Pt usage is critical for the commercialization of energy conversion devices that offer eco-friendly solutions. To achieve this goal, numerous Pt and Pt-based catalysts have been developed to reduce Pt dosage while maintaining high ORR performance, such as Pt skin-coated hollow Ag-Pt structure [1], single-atom of Pt supported on titanium nitride nanoparticles[2, 3], Pt (5 wt%)-loaded sulfur-doped zeolite-templated carbon [4], size-controlled Pt particles in nanocages [5], Pt-supported N-doped carbon nanofibers [6], Oxide-carbon composites and yttrium-doped TiO_2-C supported photo-deposit Pt nanoparticles [7], Pt monolayer/Pd/C [8], Pt_xGd/C [9], various carbon supports for Pt particles [10], etc.

Despite extensive efforts that have been made to improve the utilization efficiency of Pt as an ORR catalyst, one important issue, the size-activity relationship of the ORR on Pt, is not yet completely understood and remains a topic of great interest. For example, Bregoli demonstrated that as the diameter of Pt particle decreases from 14 nm to 3.5 nm, the specific activity towards ORR decreases and suggested that the particle size effect might be attributed to morphological changes of particles[11, 12]; A series of PtAu catalysts with different particle size were synthesized and the one with larger size showed better performance [13]; Shao and coworkers demonstrated that both mass activity and specific activity depend on the Pt particle size that the activities increase as the particle size grows from 1.3 to 2.2 nm[14] ; graphene-supported Pt single atoms follow the two-electron pathway to generate H_2O_2, while graphene-supported Pt nanoparticles prefer to a complete reduction to form H_2O [15]; Chorkendorff and the coworkers reported that the specific activity of the ORR on Pt nanoparticles decreases with decreasing particle size[16] .

While many studies have reported an increase in the specific activity with larger particle size, there are also researchers who hold the opposite view. For example, Yamamoto et al. demonstrated that the specific activity of Pt increased with decreasing particle size and that the activity of a 0.9 nm cluster is more than 10 times higher than that of 2.5 nm [17]; Hayden et al. found that the ORR-specific current density increases with increasing particle diameter up to approximately 4 nm, at which point the activity begins to level off [18].

There are debates on how particle size and other factors (such as the structure of Pt, the electrolyte, etc.) affect the catalytic ability and this has been the topic of many studies for decades. Takasu et al. suggested that the particle-size effect was attributed to larger adsorption energies due to the change in the electronic structure of smaller particles [19]; Nesselberger et al. reported that the relationship between activity and particle size is independent of the supporting electrolyte [20]; Other researchers reported that the specific activity does not depend on the particle size but the interparticle distance [21-23]; It was also reported that the electronic charge transfer effect in the electrocatalytic activity of Pt is weaker than the particle size, facet, or strain effects [24].

The wide discrepancy in ORR analysis of Pt may result from the fact that the activities of Pt were mostly measured in different environments with the interference from the adhesion that may to a certain degree affect the electron transfer between the Pt catalyst and the electrode. To address this issue, we aimed to improve the precision of Pt catalyst detection and investigate the influence of cluster size on catalytic ability. Specifically, our research focused on: (1) Use of carbon-film-based interdigitated array (IDA) electrodes with largely improved sensitivity for *in-situ* detection of reaction intermediates (H_2O_2) and provide insight into the reaction pathway and electron transfer process, instead of conventional rotating ring disk electrodes. (2) Direct synthesis of Pt catalysts onto IDA working electrodes, rather than offline preparation and pasting onto electrodes surface with the mixing of Nafion [25-27], to avoid interference from other chemicals and changes to the surface status of catalyst particles [28] [29]. Various techniques can be harnessed to directly synthesize catalysts with controlled dimensions. Examples encompass atomic layer deposition (ALD)[30, 31], which has enabled the creation of platinum (Pt) nanoparticles ranging in size from 1.3 nm to 4.6 nm on titanium dioxide nanotubes[32]; physical vapor deposition, through which palladium (Pd) particles spanning 3 to 42 nm have been fabricated on a carbon substrate[33]; dispersing method, yielding platinum particles sized at 10-100 nm[34]. The utilization of these methodologies ensures a uniform dispersion of catalyst particles across the entire electrode surface. Nevertheless, the use of IDA electrodes mandates an exacting arrangement of catalysts on the IDA generator to facilitate precise investigations of the intended catalyst.

Hence, in this study, electrochemical deposition was opted for as the technique to intricately position Pt onto the IDA generator at a micron scale. This approach enables the meticulous examination of catalytic behaviors exhibited by these Pt particles.

2. Experimental Section

2.1 Chemicals and apparatuses

Potassium ferricyanide, perchloric acid, potassium hexachloroplatinate, and sodium hydroxide were used as purchased. A scanning electron microscope (SEM) (FEI, Apreo), x-ray photoelectron spectroscopy (XPS) (Kratos Axis Ultra DLD, Al as anode material, 15 kV beam energy, 16 A/cm^2 current density), and atomic force microscope (AFM) (Asylum Research) were used for the physical characterization.

2.2 Preparation of carbon-film-based IDA electrodes and Pt catalyst

Preparation of carbon-film-based IDA electrodes. Carbon IDA electrodes were used as the working electrode and the substrate for the Pt catalyst deposition. The carbon IDA electrodes were fabricated by plating carbon-film-based patterns on Si wafer substrate, as reported in our previous work [35]. Generally, the IDA patterns were obtained through the photolithography technology, then annealed at 1100℃ in a reducing atmosphere. The IDA electrodes contain 101 electrode digits of about 2 μm width and 1000 μm length.

Preparation of Pt catalyst layer on carbon IDA electrodes. The Pt catalyst was prepared onto the carbon IDA generator through electrodeposition in aqueous solutions of 0.1 M of $HClO_4$ and various concentrations of K_2PtCl_6 (1×10^{-3} M, 1×10^{-4} M, 5×10^{-5} M, 1×10^{-5} M, 5×10^{-6} M, 1×10^{-6} M), the potential of IDA generator swept from 1.16 V to -0.2 V vs. Ag/AgCl 4 times at 0.05 V/s, and the obtained Pt samples were labeled as #1, #2, #3, #4, #5, and #6 Pt clusters, respectively. The Pt deposition on the IDA collector was processed similarly with 2.0 mM K_2PtCl_6 in order to detect the ORR intermediate (H_2O_2).

2.3 Samples characterization

Thickness of carbon film of IDA electrodes. The thickness of the carbon film is about 300 nm according to the AFM results [35].

Thickness of Pt catalyst layer on IDA electrodes. The size and thickness of the Pt catalyst layer were measured with the AFM for each sample. AFM operating mode: Tapping mode. Scan rates: 2.44 Hz. Number of pixels per line: 256.

The total surface area of platinum particles. The real surface area of Pt catalyst loaded on IDA generator was determined with the CO stripping method[36, 37], which was carried out as below: Put IDA in 0.1 M $HClO_4$ aqueous, purge pure CO and hold the potential of IDA generator at -0.166 V for 120 s to adsorb CO. Then, purge the solution with N_2 for 10 min to remove residue CO. After that, perform CO stripping cyclic voltammetry scans with IDA generator between -0.16 V and 1 V, followed by 2 additional cycles of cyclic voltammetry. No electrochemical CO oxidation can be observed in these two scans, indicating the full oxidation of adsorbed CO.

Oxygen reduction reaction. The oxygen reduction reaction was carried out in an aqueous solution of 0.1 M NaOH, which was subjected to O_2 flow for 15 min before the reaction.

In all experiments, IDA electrodes were used as the working electrodes, and carbon rod and Ag/AgCl were used as the counter electrode and reference electrode, respectively. The potential in ORR experiments was converted versus the Reversible Hydrogen Electrode (RHE).

3. Results and discussion

Carbon IDA electrodes were used as the navel tool to study the catalytic performance and reaction process of Pt-catalyzed ORR, taking advantage of its capability of *in-situ* detection and high sensitivity. The IDA electrodes are composed of two comb-like micron-size working electrodes, the generator and the collector (Fig. 1), with a collection efficiency of up to 90%.

In this work, the Pt catalyst was grown onto the IDA electrode surface directly through the electrodeposition method; the free-standing catalyst particles maintain the surface status as well as good conduct with the electrode, without any interference from the catalyst ink. So, the "true" character of the Pt catalyst can be revealed.

3.1 Characterizations of Pt-deposited IDA

As shown in Fig. 1, the two working electrodes of IDA play different roles. The carbon IDA generator is electrodeposited with Pt and performs the ORR catalytic reaction. The IDA collector is used to detect any reaction intermediate (H_2O_2) from the Pt-catalyzed ORR on the generator. To be noticed, the IDA collector was deposited with Pt as well since Pt is a good catalyst reacting with H_2O_2. So, even though both the generator and collector are loaded with Pt, only the one on the IDA generator was used as the ORR catalyst that was studied in this work, while the one on the IDA collector was for H_2O_2 detection.

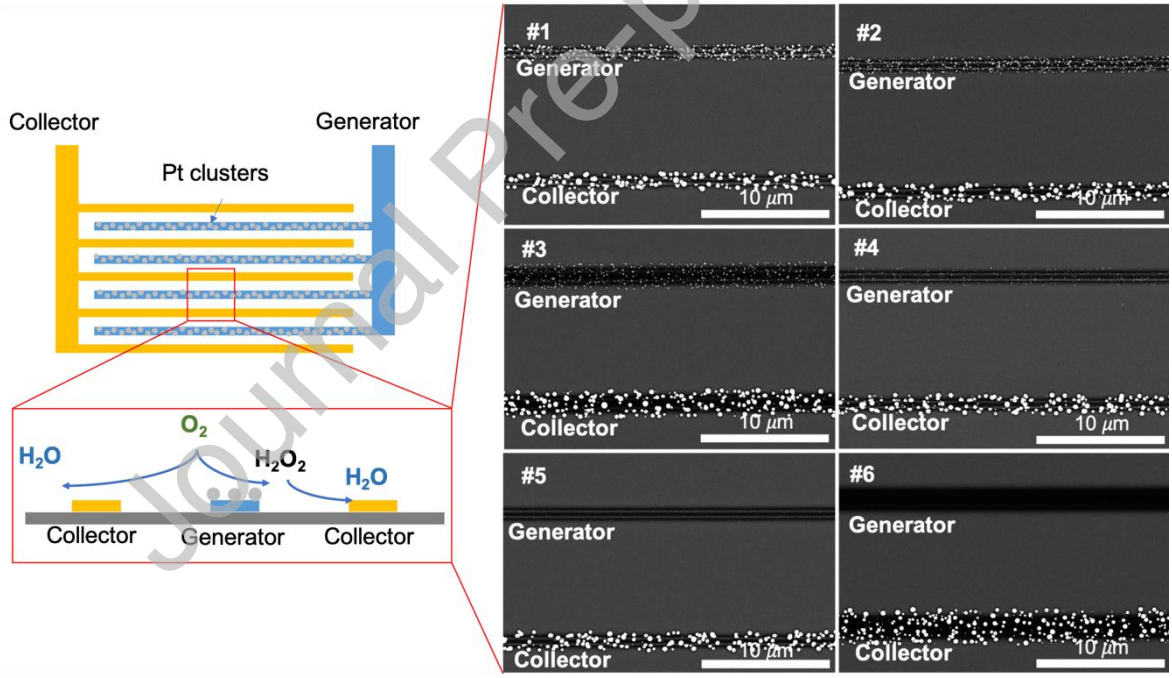

Fig. 1. Schematic diagram of IDA structure and working principle, and the SEM images of #1-#6 Pt-decorated IDA electrodes, operating voltage: 5.00 kV.

The electrodeposition of Pt catalyst onto the IDA generator were shown in Fig. 2. The humps near 0.4 and 0 V vs. Ag/AgCl are assigned to the reduction of Pt^{4+} to Pt^{2+} and the reduction of Pt^{2+} to Pt^0, respectively[38]. The deposition currents decline with the decreasing concentration of K_2PtCl_6, indicating less deposition of Pt on the electrode surface.

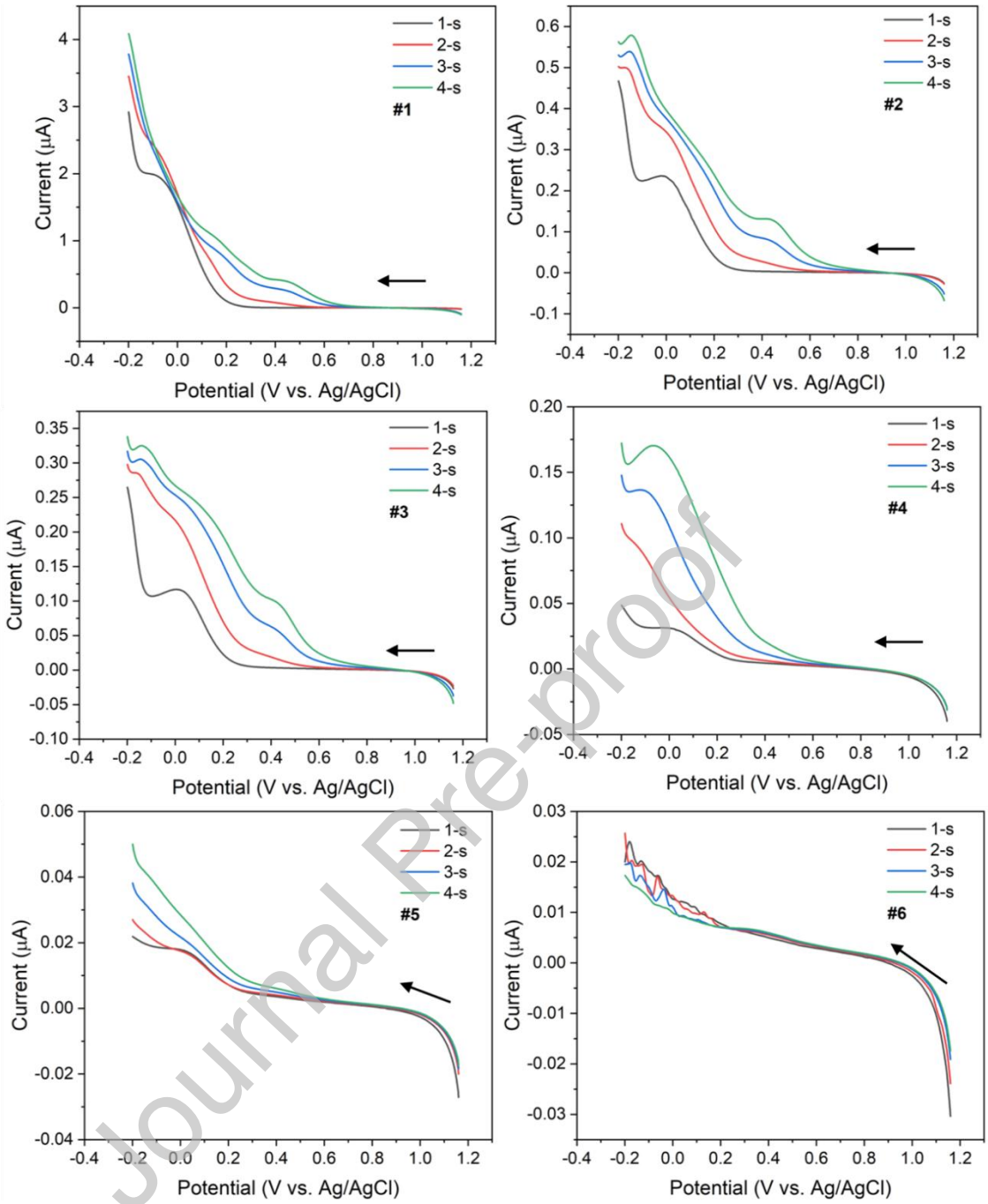

Fig. 2. The linear sweep voltammetry of Pt on IDA generators in solutions of 0.1 M of $HClO_4$ and various concentrations of K_2PtCl_6 of (a) 1×10^{-3} M, (b) 1×10^{-4} M, (3) 5×10^{-5} M, (4) 1×10^{-5} M, (5) 5×10^{-6} M, (6) 1×10^{-6} M. respectively. Ag/AgCl as the reference electrode, carbon rod as the counter electrode, scan rate of 0.05 V/s.

The IDA collector was electro-deposited with Pt as well in an aqueous solution with 2 mM K_2PtCl_6 and 0.1 M $HClO_4$, aiming at the detection of reaction intermediates (Fig. 3).

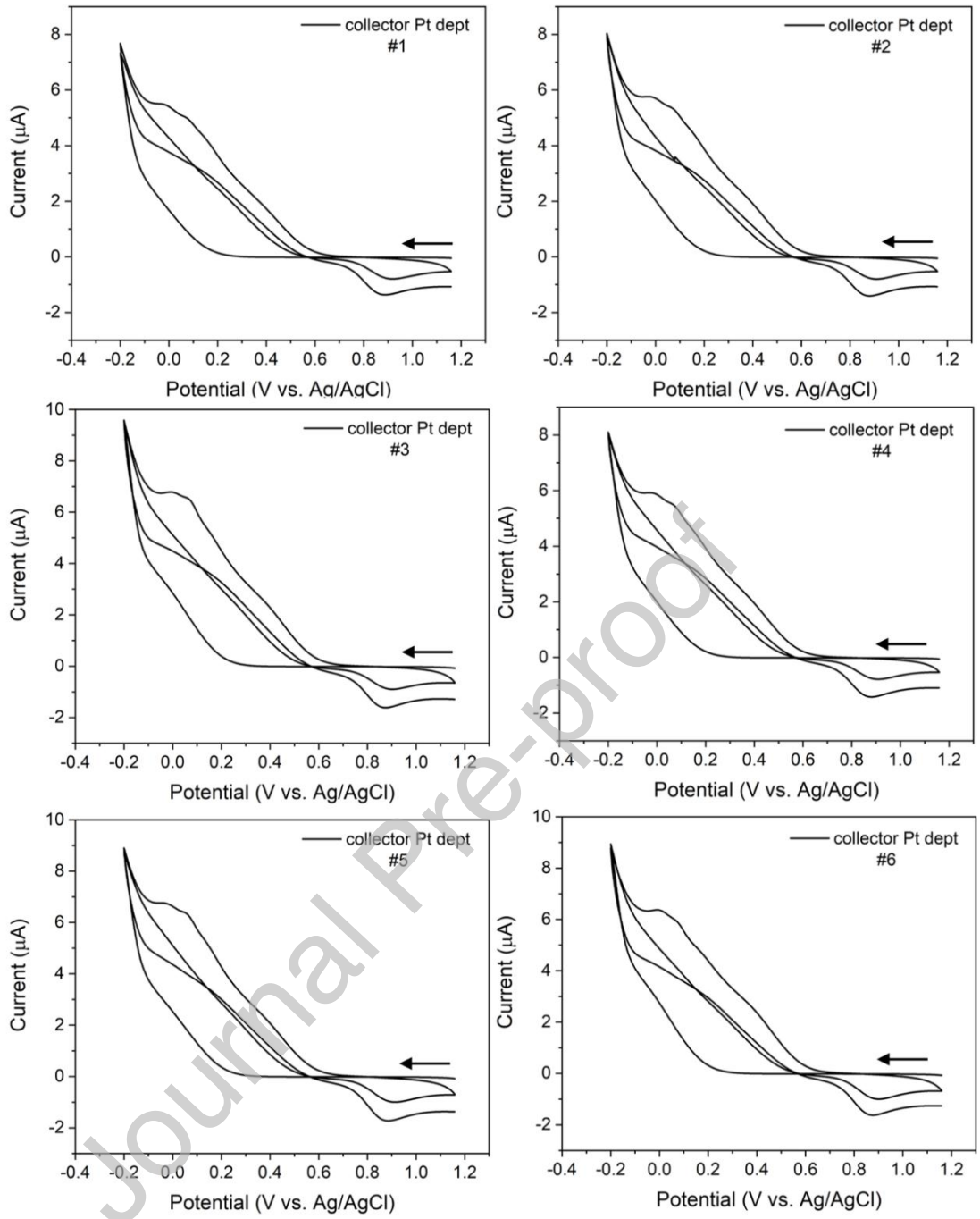

Fig. 3. The cyclic voltammetry of IDA collectors in an aqueous solution with 2 mM K_2PtCl_6 and 0.1 M $HClO_4$ for the Pt deposition. Ag/AgCl as the reference electrode, carbon rod as the counter electrode, scan rate of 0.01 V/s.

The amount of loaded Pt on each IDA generator was calculated by integrating the deposition current with time. The calculation shows that the #1 to #6 electrodes were deposited with Pt of 3.1×10^{-8} g, 6.5×10^{-9} g, 4.2×10^{-9} g, 1.6×10^{-9} g, 4.3×10^{-10} g, and 3.1×10^{-10} g, respectively. The SEM images of the Pt-loaded IDA electrodes are shown in Fig. 1. It can be seen that the size and loading density of Pt can be regulated as desired by varying the concentration of precursor; The size and loading density of Pt cluster decrease by lowering the concentration of precursor. The deposited Pt cluster is more like a cone shape, so the height of each deposited Pt cone is used to represent the size of the cluster. As shown in Fig.

4., the density of Pt clusters decreases with lower concentrations of precursor, and the height of Pt clusters change from about 60 nm to around 2.5 nm (Fig. 4).

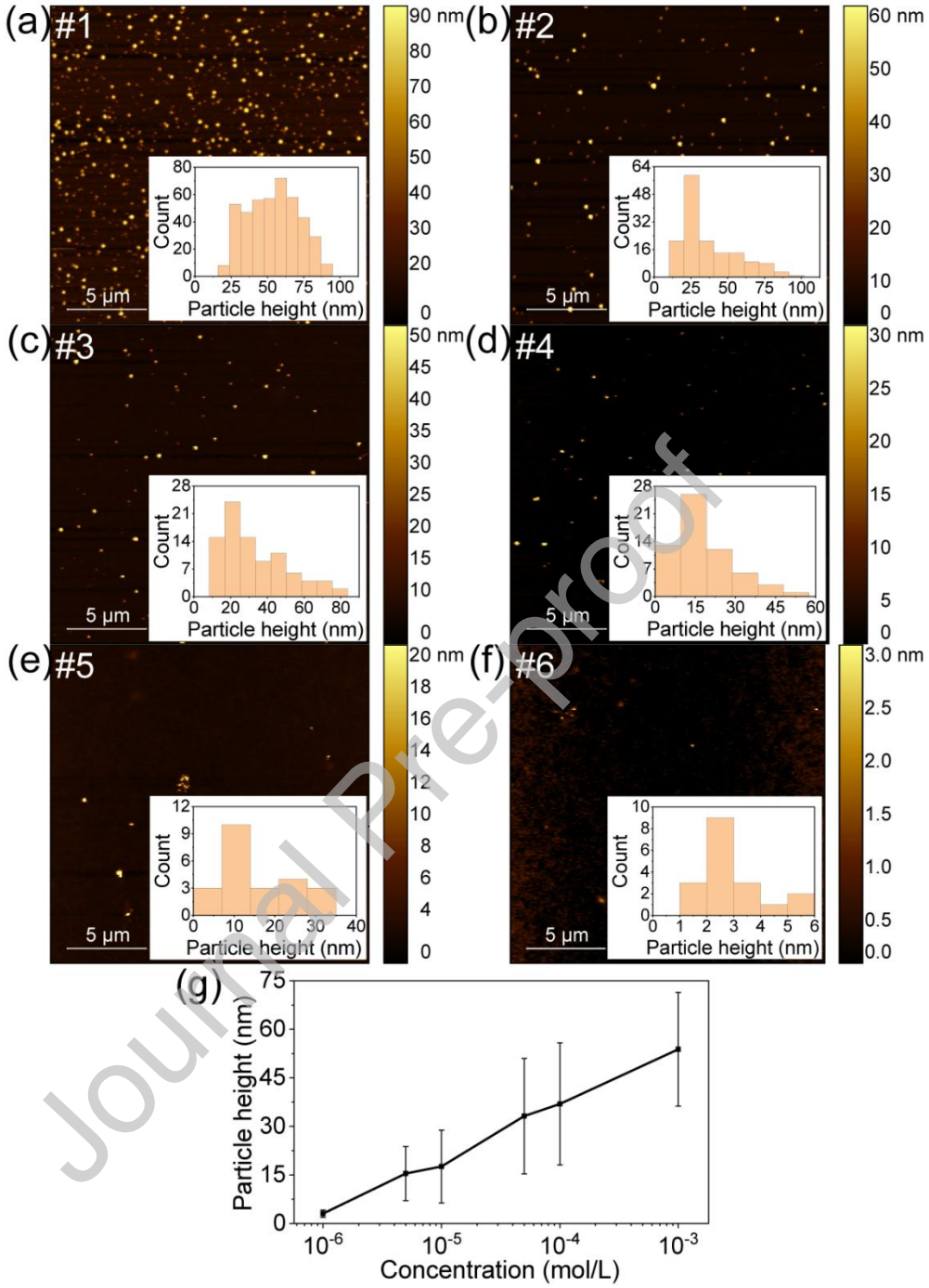

Fig. 4. The AFM image of Pt obtained from Pt precursors of different K_2PtCl_6 concentrations and the insets are statistical analyses of height of the Pt clusters from AFM result. (a) #1, (b) #2, (c) #3, (d) #4, (e) #5, (f) #6. (g) Pt particle height changes with the concentration of K_2PtCl_6. Error bars indicate the standard deviation of particle heights measured from each condition.

The valence state of the Pt was investigated using XPS (No sputtering ion beam was used in the measurement. Al was used as anode material, beam energy is 15 kV, and current density is 16 A/cm^2). And C1s peak at 284.8 eV was used to calibrate all binding energies. The typical signals of Pt 4f are shown in Fig. 5. In the case of Pt/C, the Pt 4f spectra are fitted

with three transitions corresponding to the different oxidation states of Pt (Pt^0, Pt^{2+}, and Pt^{4+}) through Avantage software, and several conditions were constrained in peak fitting analysis: The peak positions according to the references were fixed as mentioned later, FWHM (full width at half maximum) was restrained between 1 and 1.50, and the ratio of peak area between f5/2 to f7/2 is restrained roughly at 3:4. The Pt^0 $4f_{7/2}$ and Pt^0 $4f_{5/2}$ are centered at 71.60 eV and 74.95 eV, respectively. The Pt^{2+} $4f_{7/2}$ and Pt^{2+} $4f_{5/2}$ are centered at 72.40 eV and 75.75 eV, respectively. The Pt^{4+} $4f_{7/2}$ and Pt^{4+} $4f_{5/2}$ are centered at 73.90 eV and 77.25 eV, respectively [6, 17]. The XPS result suggests that the platinum clusters are mainly in the form of Pt^0 for larger-sized Pt particles, and some in the oxidized form (Pt^{2+} and Pt^{4+}). The smaller size of the clusters, the larger ratio of oxidized Pt it contains.

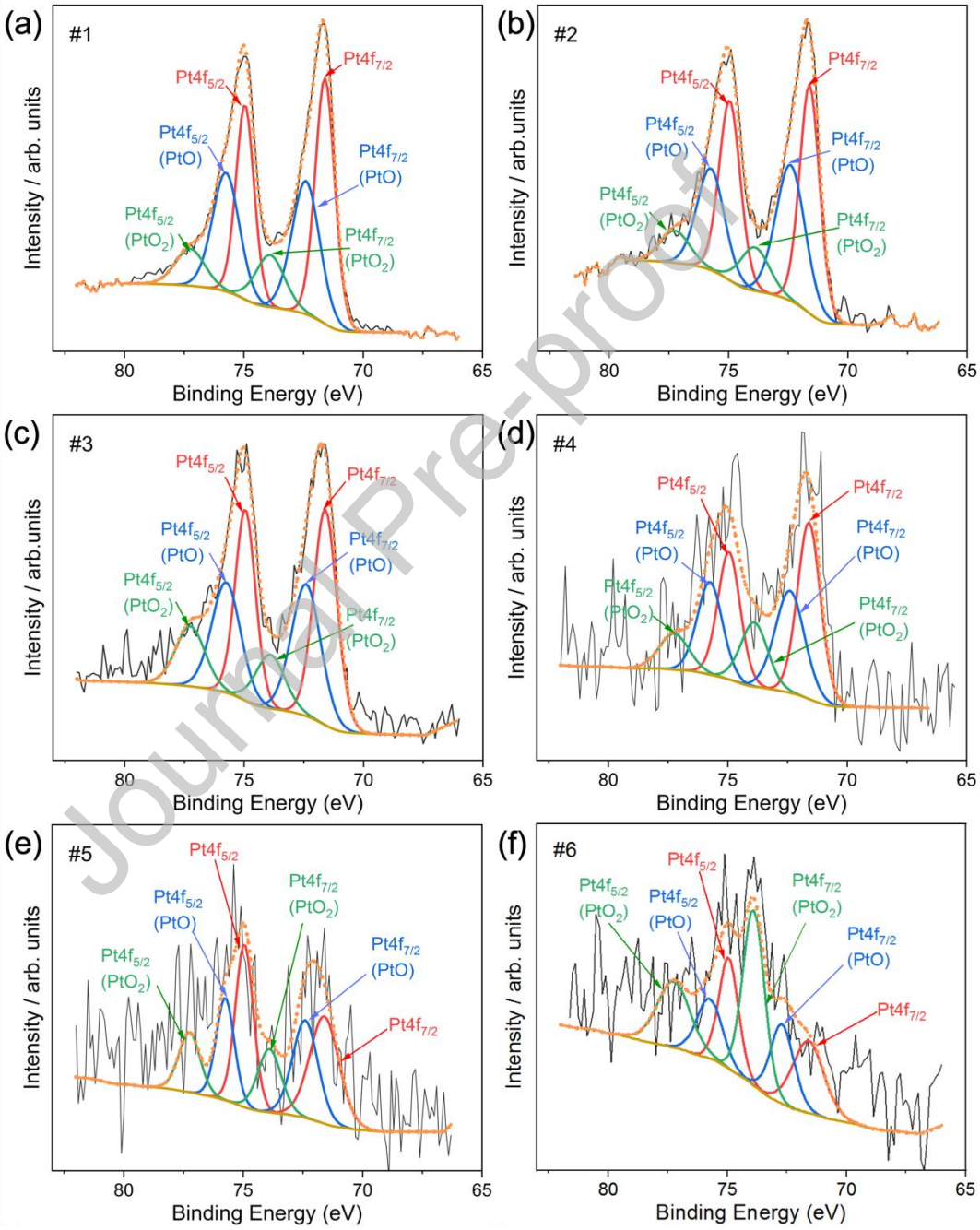

Fig. 5. The XPS Pt 4f spectra of the (a) #1, (b) #2, (c) #3, (d) #4, (5) #5 and (6) #6 samples. The background and raw data are represented as light yellow and black curves, respectively. The fitted peaks are indicated in the figures.

3.2 Electrochemical investigation

As mentioned earlier, the IDA generator-collector mode could realize the *in-situ* detection of reaction intermediates of the aimed catalytic reaction. The detection of the ORR process catalyzed by Pt with IDA generator-collector mode has been studied here, of which the specific surface area was used to calibrate the currents. For the generator, the surface areas of the deposited Pt particles were obtained through the CO stripping method [36, 39] (Fig. 6 and Table 1), the generator current was then divided by the total surface area of Pt particles, obtaining the generator current density (current per unit surface area of Pt particles), which is also known as the specific activity.

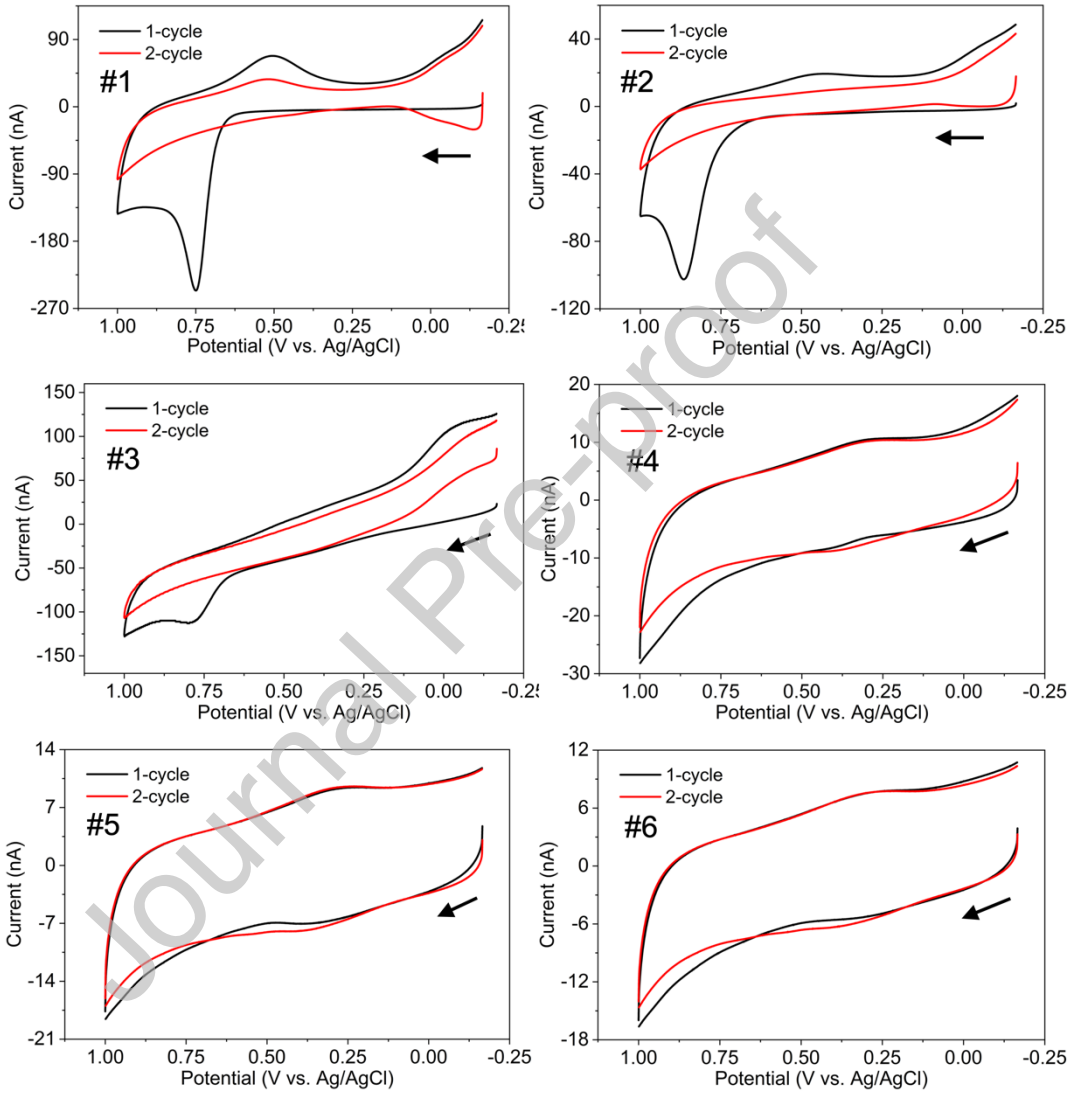

Fig. 6. The cyclic voltammetry of Pt-loaded IDA generator in 0.1 M $HClO_4$ aqueous solution saturated with CO, Ag/AgCl as the reference electrode, carbon rod as the counter electrode, scan rate of 0.1 V/s.

Table 1. Calculated total surfaces of Pt particles for different samples.

	#1	#2	#3	#4	#5	#6
Areas of Pt particles /cm^2	0.013	0.0055	0.0025	0.00076	0.00024	0.00022

Taking the #1 Pt as an example (Fig. 7a), the generator current density starts to rise sharply at around 0.9 V, indicating a fast reduction of O_2 on the IDA generator. Then, it reaches the maximum at around 0.62 V and keeps at a steady state, representing a diffusion-controlled current at the region. All other samples have been investigated with ORR, as show in Fig. 7(b)-(f). Three things worth noticing from the result: 1) With the decreasing loading amount and Pt particle size, the specific activity of the Pt catalyst on the IDA generator increases, indicating that a larger number of active sites per unit area becomes accessible for the smaller-sized Pt particles in comparison to their larger counterparts. 2) At the potential lower than 0.6 V, the catalytic current (current on the generator) converts from the diffusion control to the mixed diffusion-kinetic control, which can be explained as the change of mass transfer near the electrode surface, i.e. both efficient mass transfer and catalytic ability contribute to the catalytic current obtained from the smaller size and looser distributed Pt catalysts. 3) The observed onset potential of the catalytic reaction moves towards the negative direction for the smaller-size Pt catalysts. Taking the potential at which 10% of its maximum current density obtained as the onset overpotential, as summarized in the inset in Fig. 7(g), the overpotential is larger for the smaller-sized Pt catalysts. A possible reason is that the smaller size and less density of Pt would generate a larger amount of oxidized Pt per unit mass of the catalyst, the oxidized Pt on the electrode surface may block the adsorption of O_2 to the catalyst surface [40], and result in a larger overpotential.

The production of H_2O_2 was tracked through the IDA collector (Fig. 7), here the collector current was divided by the Pt cluster area as well, indicating the H_2O_2 produced by the unit area of Pt. The collector current changes along with the reduction of O_2 on the generator. For the larger-sized Pt, the production of H_2O_2 is relatively low and shows a peak at around 0.7 V. For the smaller-sized Pt, the collector current keeps increasing with the reduction reaction of O_2, indicating a continuous and relatively large production of H_2O_2 from the ORR.

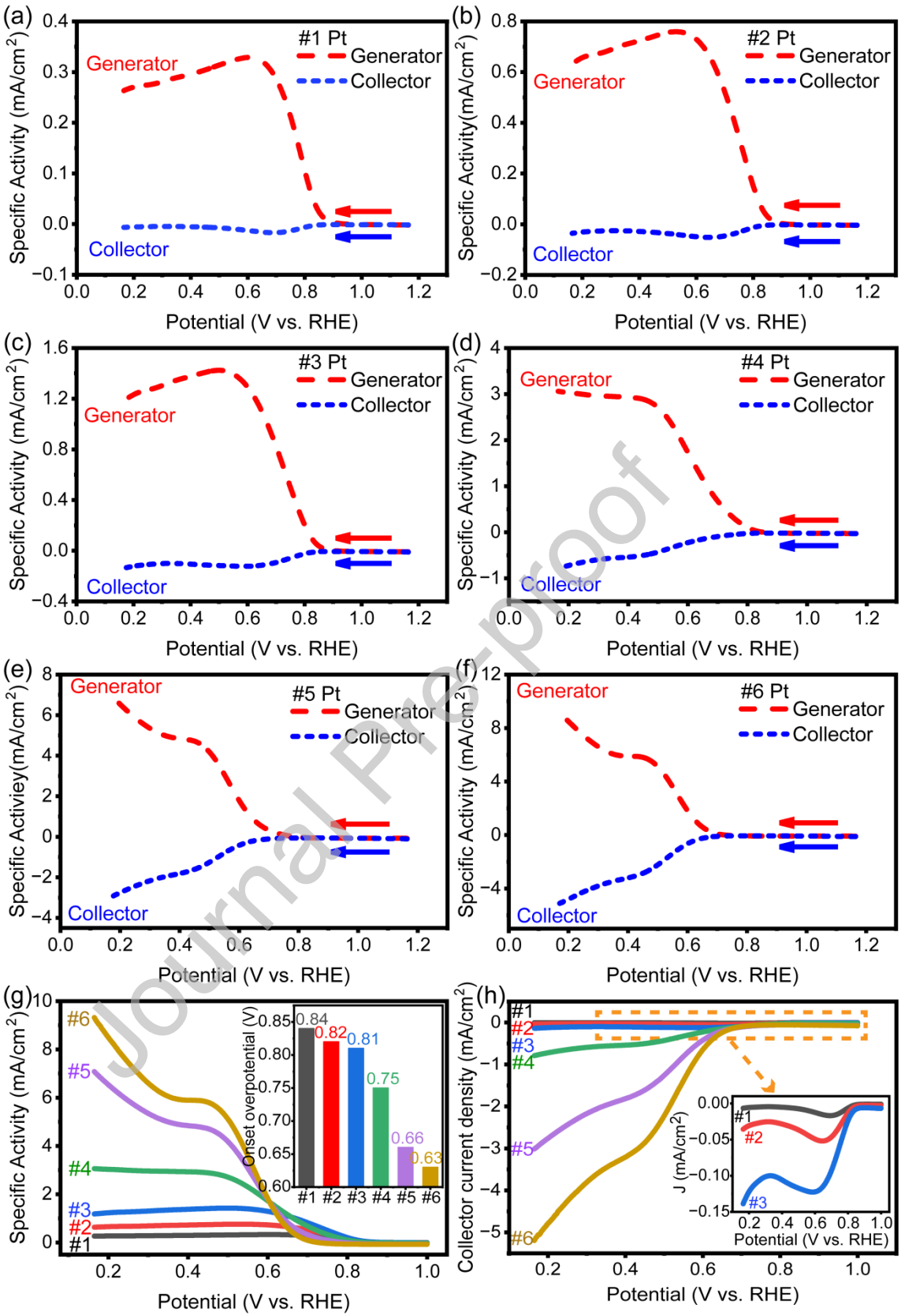

Fig 7. The current density of the ORR with generator-collector mode in 0.1M NaOH aqueous solution. (a)-(f) represent the #1-#6 samples, respectively. (g) and (h) represent the comparison of all generator currents and all collector currents, respectively, the inset is the

onset overpotential of different Pt samples. The potential of generator scans and the potential of collector is at 1.2 V vs. RHE.

Mass activity is calculated by dividing currents by the specific mass of catalysts. As shown in Fig. 8, the generator current increases, and the collector current increases along with it when sweeping the potential to the negative direction. Comparing all six Pt samples' mass activities, it shows that the smaller the cluster size, the larger the mass activity and the collector currents. The yield of H_2O_2 increases with the smaller-size Pt particles.

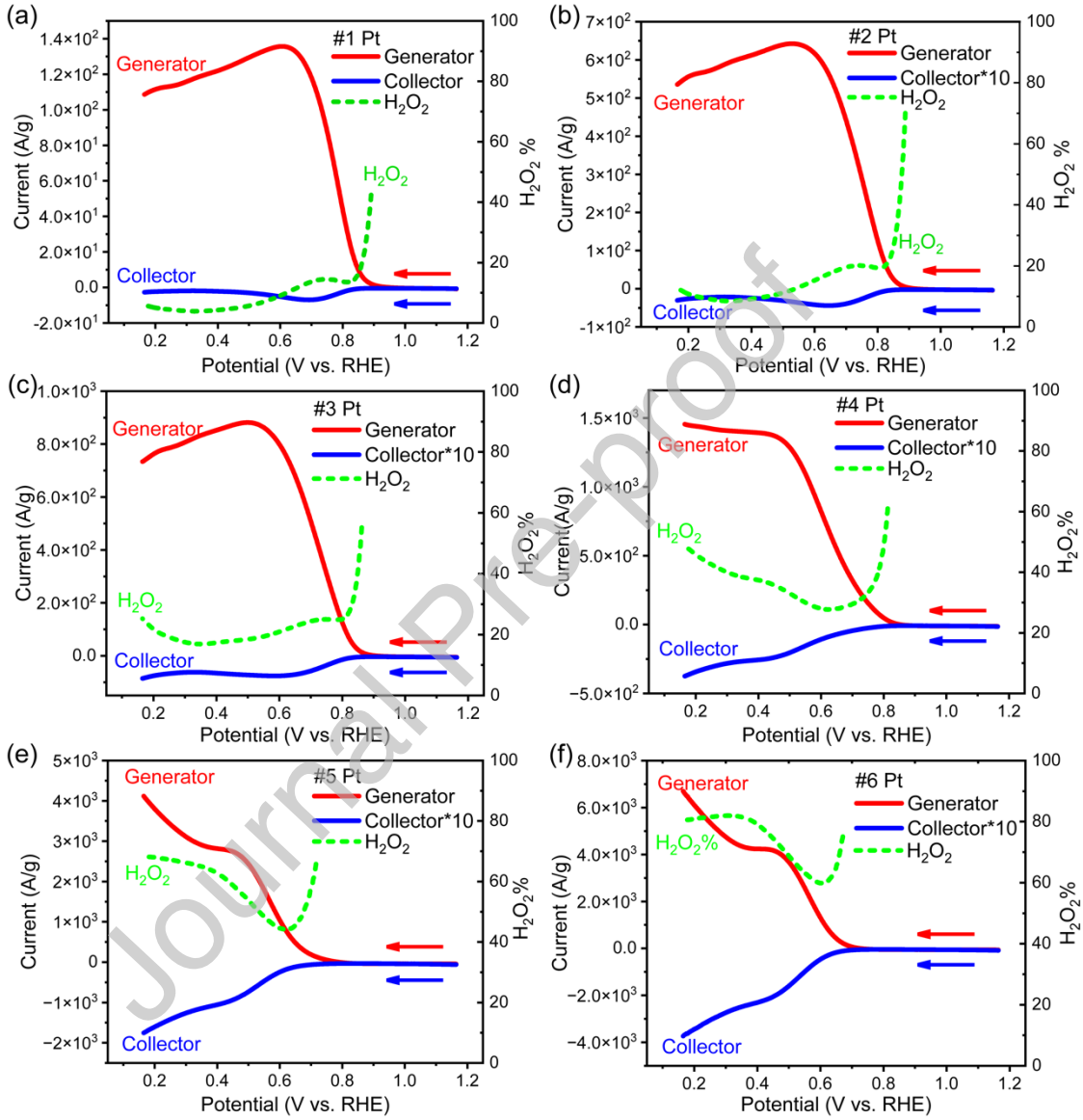

Fig. 8. The mass activity of the different Pt catalysts towards ORR. (a)-(f) are the current response with the generator-collector mode and the percent yield of H_2O_2 for the #1 - #6 samples. 0.1M NaOH aqueous solution was used for ORR. The potential of generator scans and the potential of collector is at 1.2 V vs. RHE.

The generator currents and collector currents were compared in detail in Fig. 9. For the generator currents, two distinguishing features should be noticed: 1) Overpotential. ORR catalyzed with Pt of smaller size shows larger overpotential than the one with larger particle size, which is in accordance with the previous report [18]. For example, the catalytic current starts to increase at 0.9 V vs. RHE for the #1 Pt (larger-sized Pt), and it is 0.7 V vs. RHE for

the #6 Pt (smaller-sized Pt). As mentioned earlier, the larger overpotential may result from the larger oxidized surface for the smaller-sized Pt. 2) Mass activity. A larger size leads to lower mass activity. Taking the currents at the potential of onset overpotential plus 0.03 V as an example (the kinetic-controlled region), the current for #2 to #6 Pt particles (which are 142.0 A/g, 183.8 A/g, 234.6 A/g, 680.9 A/g and 1242.5 A/g, respectively) enhanced to 4.2 times, 5.5 times, 7.0 times, 20.4 times and 37.2 times, respectively, compared with the current of #1 Pt (33.4 A/g), while the particle height decrease from about 60 nm to 2.5 nm. The larger mass activity of catalysts with smaller particle sizes results from the increased active sites that are exposed to the solution. For the collector, the current on it represents the oxidation of H_2O_2. As we can see, the collector current starts to increase along with the ongoing O_2 reduction on the IDA generator. The small-sized Pt shows a large current per unit mass, which means more H_2O_2 is generated from the ORR. Taking the collector currents at the potential of onset overpotential plus 0.03 V as an example, it increased 227 times when Pt cluster sizes decrease from the #1 to #6 sample, indicating a largely generated H_2O_2 with smaller-sized Pt particles. Compared with the increase of mass activity on the IDA generator for smaller-sized Pt clusters, the current change on the collector (the production of H_2O_2) is much more significant. Based on the current analysis, it can be inferred that the rise in collector current (the generation of H_2O_2) is not solely due to the increase in active sites when smaller-sized Pt particles are used. Rather, it is also likely attributed to a shift in reaction pathways, potentially favoring the 2-electron pathway over the 4-electron pathway. This shift could result in an enhanced production of H_2O_2. Fig. 9(c-d) summarizes the percentage production of H_2O_2 and the corresponding average electron transfer number (n) for ORR. Large-sized Pt shows an *n* of about 4 and H_2O_2% of less than 10%. The smaller the particle size, the lower the *n* and the higher the H_2O_2%.

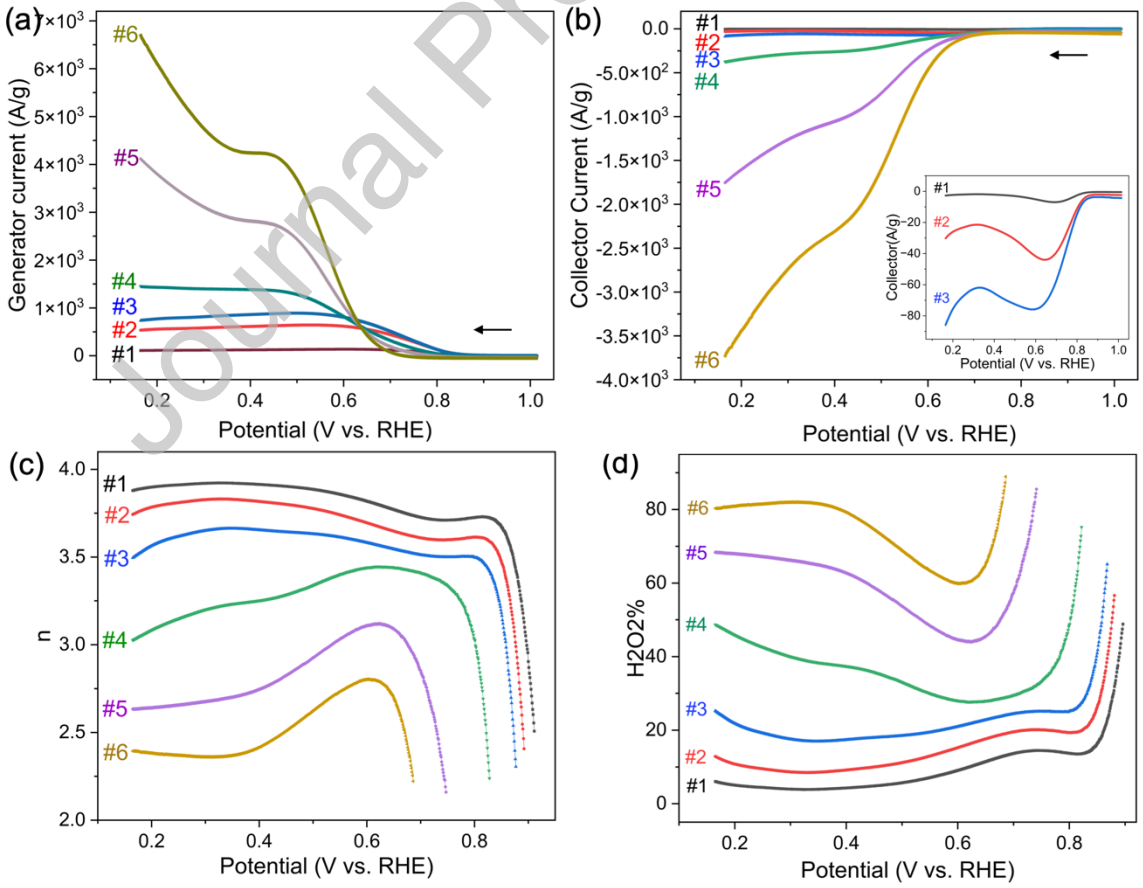

Fig. 9. The comparison of all the generator currents (a), all the collector currents (b), all the electron transfer numbers (c), and all the percentage yield of H_2O_2 of all #1-#6 samples (d).

Fig.10(a) shows the Tafel plots derived from the ORR catalytic reaction on IDA generator. The Pt catalyst with relatively large particle sizes shows small Tafel slopes of 60 mV/decade, 57 mV/decade, and 59 mV/decade for the #1, #2, and #3 Pt catalyst, respectively. This current region corresponds to the Temkin isotherm adsorption of O_2, where the adsorbed hydroxyl species at the Pt surface determines the electrode activity[25]. For the Pt particles with smaller sizes, the related Tafel slopes are found to split into two parts: At the low overpotential region, it shows the same Tafel slope as the one of large-sized Pt, around 60 mV/decade; At the high overpotential region, the Tafel slope increases to 109-132 mV/dec. The Langmuir isotherm (low coverage of O_2) at high overpotential is commonly interpreted as a two-electron transfer reaction as the rate-determining step [41-43]. This result is in accordance with the IDA results shown in Fig. 7 and 8.

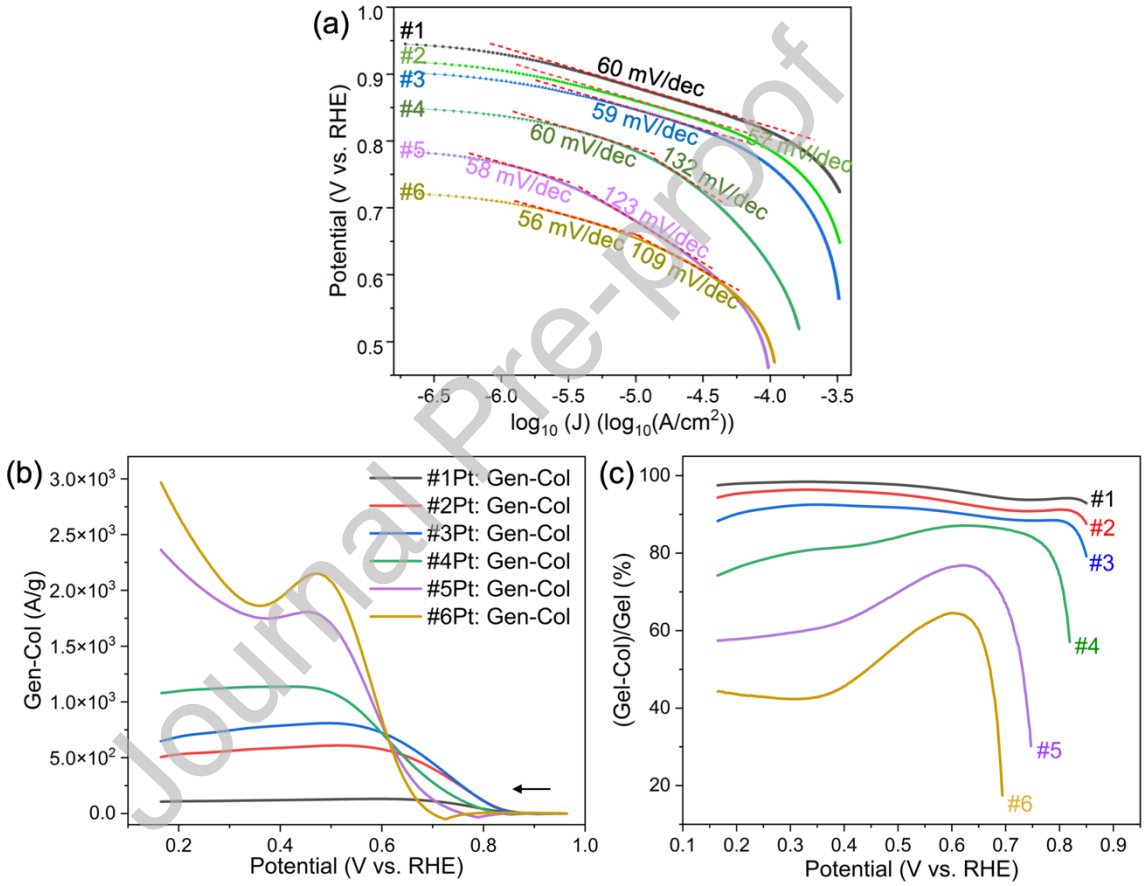

Fig. 10. (a)The Tafel plot of ORR for #1-#6 samples; (b) The difference of generator and collector currents (labeled as "Gen-Col") of all #1-#6 samples; (c) The percentage of the difference of generator and collector currents in all generator currents, i.e. the percentage of "pure" 4-electron pathway for all #1-#6 samples.

Notably, the difference between the generator current and collector current was calculated, and found interesting results. As demonstrated earlier, the generator current represents the total catalytic currents, i.e. the current caused by all the electrons transferred through the reaction, which includes the possible 2-electron-transfer reaction with the production of H_2O_2, the 4-electron-transfer reaction process with the production of H_2O, and any other possible side reactions. Suppose the real reaction is a simple combination of a certain amount of "pure"

2-electron-transfer reaction and a certain amount of "pure" 4-electron-transfer reaction, since the collector current is the direct reflection of the 2-electron-transfer process, then by subtracting the collector current from the generator current, the leftover generator current would represent the "pure" 4-electron-transfer process. As shown in Fig. 10(b), smaller-sized Pt catalyzes ORR that undergoes more 4-electron-transfer process than 2-electron-transfer process, catalyzed by unit mass of catalyst. Furthermore, the "pure" 4-electron-transfer current (i.e. generator current subtracts collector current) divides by the total catalytic current (i.e. the generator current) gives the percentage of "pure 4-electron-transfer current" to the total current, as shown in Fig. 10(c). In summary, the IDA results provide a comprehensive understanding of the total catalytic currents and the reaction process for the Pt catalysts of different sizes. Specifically, the smaller-sized Pt exhibits a greater total catalytic current and a higher percentage yield of H_2O_2 compared to the larger-sized Pt. Further analysis of the IDA results reveals that the ORR catalytic current catalyzed by the smaller-sized Pt (#6) is contributed by approximately 45% of the 4-electron pathway and 55% of the 2-electron pathway, while the ORR catalyzed by the larger-sized Pt (#1) mainly follows the 4-electron pathway with a nearly 100% contribution.

4. Conclusion

The size effect of Pt particles on catalyzing ORR has been carefully examined with a special tool of IDA electrodes. The use of IDA electrodes shows two advantages: 1) the direct transfer of electrons between catalyst and electrode was realized without the involvement of the catalyst adhesion and the possible effect from it. 2) high collection efficiency of IDA enables more sensitive *in situ* detection of H_2O_2 since the collection efficiency of IDA (above 80%) is largely improved than RRDE (around 30%). The ORR process catalyzed with Pt particles of different sizes and the corresponding H_2O_2 production were analyzed with IDA. Based on the analysis, the study concludes that the specific activity and mass activity of Pt catalyst decrease with increasing particle size. The overpotential of ORR catalyzed by smaller-sized Pt is higher than that by larger-sized Pt. The smaller-sized Pt catalyzed ORR shows a lower proportion of the 4-electron pathway compared to the larger-sized Pt, and vice versa.

Acknowledgments

This research was supported by the State Key Laboratory of Multiphase Flow in Power Engineering, the Natural Science Basic Research Program of Shaanxi (Program No. 2023-JC-YB-116), and the National Natural Science Foundation of China (No. 51702250).

Reference

[1] T. Fu, J. Huang, S. Lai, S. Zhang, J. Fang, J. Zhao, Pt skin coated hollow Ag-Pt bimetallic nanoparticles with high catalytic activity for oxygen reduction reaction, J. Power Sources, 365 (2017) 17-25. https://doi.org/10.1016/j.jpowsour.2017.08.066

[2] S. Yang, J. Kim, Y.J. Tak, A. Soon, H. Lee, Single-Atom Catalyst of Platinum Supported on Titanium Nitride for Selective Electrochemical Reactions, Angew. Chem. Int. Ed. Engl., 55 (2016) 2058-2062. https://doi.org/10.1002/anie.201509241

[3] R.Q. Zhang, T.H. Lee, B.D. Yu, C. Stampfl, A. Soon, The role of titanium nitride supports for single-atom platinum-based catalysts in fuel cell technology, Phys. Chem. Chem. Phys., 14 (2012) 16552-16557. https://doi.org/10.1039/c2cp41392b

[4] C.H. Choi, M. Kim, H.C. Kwon, S.J. Cho, S. Yun, H.-T. Kim, K.J.J. Mayrhofer, H. Kim, M. Choi, Tuning selectivity of electrochemical reactions by atomically dispersed platinum catalyst, Nat. Commun., 7 (2016) 10922. https://doi.org/10.1038/ncomms10922

[5] K. Yamamoto, T. Imaoka, W.J. Chun, O. Enoki, H. Katoh, M. Takenaga, A. Sonoi, Size-specific catalytic activity of platinum clusters enhances oxygen reduction reactions, Nat Chem, 1 (2009) 397-402. https://doi.org/10.1038/nchem.288
[6] J. Melke, B. Peter, A. Habereder, J. Ziegler, C. Fasel, A. Nefedov, H. Sezen, C. Woll, H. Ehrenberg, C. Roth, Metal-Support Interactions of Platinum Nanoparticles Decorated N-Doped Carbon Nanofibers for the Oxygen Reduction Reaction, ACS Appl Mater Interfaces, 8 (2016) 82-90. https://doi.org/10.1021/acsami.5b06225
[7] L.A. Estudillo-Wong, Y. Luo, J.A. Díaz-Real, N. Alonso-Vante, Enhanced oxygen reduction reaction stability on platinum nanoparticles photo-deposited onto oxide-carbon composites, Applied Catalysis B: Environmental, 187 (2016) 291-300. https://doi.org/10.1016/j.apcatb.2016.01.030
[8] G. Chen, K.A. Kuttiyiel, M. Li, D. Su, L. Du, C. Du, Y. Gao, W. Fei, G. Yin, K. Sasaki, R.R. Adzic, Correlating the electrocatalytic stability of platinum monolayer catalysts with their structural evolution in the oxygen reduction reaction, Journal of Materials Chemistry A, 6 (2018) 20725-20736. https://doi.org/10.1039/c8ta06686h
[9] C.A. Campos-Roldán, F. Pailloux, P.-Y. Blanchard, D.J. Jones, J. Rozière, S. Cavaliere, Rational Design of Carbon-Supported Platinum–Gadolinium Nanoalloys for Oxygen Reduction Reaction, ACS Catalysis, 11 (2021) 13519-13529. https://doi.org/10.1021/acscatal.1c02449
[10] A. Bharti, G. Cheruvally, Influence of various carbon nano-forms as supports for Pt catalyst on proton exchange membrane fuel cell performance, J. Power Sources, 360 (2017) 196-205. https://doi.org/10.1016/j.jpowsour.2017.05.117
[11] L.J. Bregoli, The influence of platinum crystallite size on the electrochemical reduction of oxygen in phosphoric acid, Electrochim. Acta, 23 (1978) 489-492. https://doi.org/https://doi.org/10.1016/0013-4686(78)85025-7
[12] M.L. Sattler, P.N. Ross, The surface structure of Pt crystallites supported on carbon black, Ultramicroscopy, 20 (1986) 21-28. https://doi.org/https://doi.org/10.1016/0304-3991(86)90163-4
[13] S. Yin, Z. Xie, X. Deng, W. Xuan, Y. Duan, S. Zhang, Y. Liang, Simple synthesis of ordered platinum-gold nanoparticles with the enhanced catalytic activity for oxygen reduction reaction, J. Electroanal. Chem., 856 (2020). https://doi.org/10.1016/j.jelechem.2019.113707
[14] M. Shao, A. Peles, K. Shoemaker, Electrocatalysis on platinum nanoparticles: particle size effect on oxygen reduction reaction activity, Nano Lett., 11 (2011) 3714-3719. https://doi.org/10.1021/nl2017459
[15] X. Song, N. Li, H. Zhang, H. Wang, L. Wang, Z. Bian, Promotion of hydrogen peroxide production on graphene-supported atomically dispersed platinum: Effects of size on oxygen reduction reaction pathway, J. Power Sources, 435 (2019). https://doi.org/10.1016/j.jpowsour.2019.226771
[16] F.J. Perez-Alonso, D.N. McCarthy, A. Nierhoff, P. Hernandez-Fernandez, C. Strebel, I.E. Stephens, J.H. Nielsen, I. Chorkendorff, The effect of size on the oxygen electroreduction activity of mass-selected platinum nanoparticles, Angew. Chem. Int. Ed. Engl., 51 (2012) 4641-4643. https://doi.org/10.1002/anie.201200586
[17] K. Yamamoto, T. Imaoka, W.-J. Chun, O. Enoki, H. Katoh, M. Takenaga, A. Sonoi, Size-specific catalytic activity of platinum clusters enhances oxygen reduction reactions, Nature Chemistry, 1 (2009) 397-402. https://doi.org/10.1038/nchem.288
[18] A. Anastasopoulos, J.C. Davies, L. Hannah, B.E. Hayden, C.E. Lee, C. Milhano, C. Mormiche, L. Offin, The particle size dependence of the oxygen reduction reaction for

carbon-supported platinum and palladium, ChemSusChem, 6 (2013) 1973-1982. https://doi.org/10.1002/cssc.201300208
[19] Y. Takasu, N. Ohashi, X.G. Zhang, Y. Murakami, H. Minagawa, S. Sato, K. Yahikozawa, Size effects of platinum particles on the electroreduction of oxygen, Electrochim. Acta, 41 (1996) 2595-2600. https://doi.org/https://doi.org/10.1016/0013-4686(96)00081-3
[20] M. Nesselberger, S. Ashton, J.C. Meier, I. Katsounaros, K.J. Mayrhofer, M. Arenz, The particle size effect on the oxygen reduction reaction activity of Pt catalysts: influence of electrolyte and relation to single crystal models, J. Am. Chem. Soc., 133 (2011) 17428-17433. https://doi.org/10.1021/ja207016u
[21] M. Watanabe, H. Sei, P. Stonehart, The influence of platinum crystallite size on the electroreduction of oxygen, Journal of Electroanalytical Chemistry and Interfacial Electrochemistry, 261 (1989) 375-387. https://doi.org/https://doi.org/10.1016/0022-0728(89)85006-5
[22] H. Yano, J. Inukai, H. Uchida, M. Watanabe, P.K. Babu, T. Kobayashi, J.H. Chung, E. Oldfield, A. Wieckowski, Particle-size effect of nanoscale platinum catalysts in oxygen reduction reaction: an electrochemical and 195Pt EC-NMR study, Phys. Chem. Chem. Phys., 8 (2006) 4932-4939. https://doi.org/10.1039/b610573d
[23] M. Nesselberger, M. Roefzaad, R.F. Hamou, P.U. Biedermann, F.F. Schweinberger, S. Kunz, K. Schloegl, G.K. Wiberg, S. Ashton, U. Heiz, K.J. Mayrhofer, M. Arenz, The effect of particle proximity on the oxygen reduction rate of size-selected platinum clusters, Nat Mater, 12 (2013) 919-924. https://doi.org/10.1038/nmat3712
[24] X. Wang, Y. Orikasa, Y. Uchimoto, Platinum-Based Electrocatalysts for the Oxygen-Reduction Reaction: Determining the Role of Pure Electronic Charge Transfer in Electrocatalysis, ACS Catalysis, 6 (2016) 4195-4198. https://doi.org/10.1021/acscatal.6b00497
[25] <~~Single-Wall Carbon Nanotubes Supported Platinum Nanoparticles with Improved Electrocatalytic Activity for ORR.pdf>.
[26] M.F. Labata, G. Li, J. Ocon, P.-Y.A. Chuang, Insights on platinum-carbon catalyst degradation mechanism for oxygen reduction reaction in acidic and alkaline media, J. Power Sources, 487 (2021). https://doi.org/10.1016/j.jpowsour.2020.229356
[27] J. Melke, B. Peter, A. Habereder, J. Ziegler, C. Fasel, A. Nefedov, H. Sezen, C. Wöll, H. Ehrenberg, C. Roth, Metal–Support Interactions of Platinum Nanoparticles Decorated N-Doped Carbon Nanofibers for the Oxygen Reduction Reaction, ACS Applied Materials & Interfaces, 8 (2016) 82-90. https://doi.org/10.1021/acsami.5b06225
[28] D.M. Drew C. Higgins, Zhongwei Chen, Nitrogen-Doped Carbon Nanotubes as Platinum Catalyst Supports for Oxygen Reduction Reaction in Proton Exchange Membrane Fuel Cells, Journal of Physical Chemistry C, 114 (2010) 7. https://doi.org/https://doi.org/10.1021/jp106814j
[29] C. Kim, J.-G. Oh, Y.-T. Kim, H. Kim, H. Lee, Platinum dendrites with controlled sizes for oxygen reduction reaction, Electrochem. Commun., 12 (2010) 1596-1599. https://doi.org/10.1016/j.elecom.2010.09.004
[30] S.M. Thalluri, J. Rodriguez-Pereira, R. Zazpe, B. Bawab, E. Kolíbalová, L. Jelinek, J.M. Macak, Enhanced C-O Functionality on Carbon Papers Ensures Lowering Nucleation Delay of ALD for Ru towards Unprecedented Alkaline HER Activity, Small, 19 (2023) 2300974. https://doi.org/https://doi.org/10.1002/smll.202300974
[31] J.S. King, A. Wittstock, J. Biener, S.O. Kucheyev, Y.M. Wang, T.F. Baumann, S.K. Giri, A.V. Hamza, M. Baeumer, S.F. Bent, Ultralow Loading Pt Nanocatalysts Prepared by Atomic Layer

Deposition on Carbon Aerogels, Nano Lett., 8 (2008) 2405-2409. https://doi.org/10.1021/nl801299z
[32] V.C. Anitha, R. Zazpe, M. Krbal, J. Yoo, H. Sopha, J. Prikryl, G. Cha, S. Slang, P. Schmuki, J.M. Macak, Anodic TiO2 nanotubes decorated by Pt nanoparticles using ALD: An efficient electrocatalyst for methanol oxidation, J. Catal., 365 (2018) 86-93. https://doi.org/https://doi.org/10.1016/j.jcat.2018.06.017
[33] W. Liu, Y. Magnin, D. Förster, J. Bourgon, T. Len, F. Morfin, L. Piccolo, H. Amara, C. Zlotea, Size-dependent hydrogen trapping in palladium nanoparticles, Journal of Materials Chemistry A, 9 (2021) 10354-10363. https://doi.org/10.1039/D0TA12174F
[34] K. Bergamaski, A.L. Pinheiro, E. Teixeira-Neto, F.C. Nart, Nanoparticle size effects on methanol electrochemical oxidation on carbon supported platinum catalysts, J. Phys. Chem. B, 110 (2006) 19271-19279. https://doi.org/10.1021/jp063337h
[35] F. Liu, G. Kolesov, B.A. Parkinson, Preparation, Applications, and Digital Simulation of Carbon Interdigitated Array Electrodes, Anal. Chem., 86 (2014) 7391-7398. https://doi.org/10.1021/ac5019364
[36] T.R. Garrick, T.E. Moylan, M.K. Carpenter, A. Kongkanand, Editors' Choice—Electrochemically Active Surface Area Measurement of Aged Pt Alloy Catalysts in PEM Fuel Cells by CO Stripping, J. Electrochem. Soc., 164 (2016) F55-F59. https://doi.org/10.1149/2.0381702jes
[37] S. Rudi, C. Cui, L. Gan, P. Strasser, Comparative Study of the Electrocatalytically Active Surface Areas (ECSAs) of Pt Alloy Nanoparticles Evaluated by Hupd and CO-stripping voltammetry, Electrocatalysis, 5 (2014) 408-418. https://doi.org/10.1007/s12678-014-0205-2
[38] A.C. Hill, R.E. Patterson, J.P. Sefton, M.R. Columbia, Effect of Pb(II) on the Morphology of Platinum Electrodeposited on Highly Oriented Pyrolytic Graphite, Langmuir, 15 (1999) 4005-4010. https://doi.org/10.1021/la981291g
[39] E.G. Ciapina, S.F. Santos, E.R. Gonzalez, Electrochemical CO stripping on nanosized Pt surfaces in acid media: A review on the issue of peak multiplicity, J. Electroanal. Chem., 815 (2018) 47-60. https://doi.org/10.1016/j.jelechem.2018.02.047
[40] I. Katsounaros, W.B. Schneider, J.C. Meier, U. Benedikt, P.U. Biedermann, A.A. Auer, K.J. Mayrhofer, Hydrogen peroxide electrochemistry on platinum: towards understanding the oxygen reduction reaction mechanism, Phys. Chem. Chem. Phys., 14 (2012) 7384-7391. https://doi.org/10.1039/c2cp40616k
[41] J. Xu, P. Gao, T.S. Zhao, Non-precious Co3O4 nano-rod electrocatalyst for oxygen reduction reaction in anion-exchange membrane fuel cells, Energy Environ. Sci., 5 (2012) 5333-5339. https://doi.org/10.1039/C1EE01431E
[42] B. Liu, A.J. Bard, Scanning Electrochemical Microscopy. 45. Study of the Kinetics of Oxygen Reduction on Platinum with Potential Programming of the Tip, The Journal of Physical Chemistry B, 106 (2002) 12801-12806. https://doi.org/10.1021/jp026824f
[43] Z.-s. Yin, T.-h. Hu, J.-l. Wang, C. Wang, Z.-x. Liu, J.-w. Guo, Preparation of highly active and stable polyaniline-cobalt-carbon nanotube electrocatalyst for oxygen reduction reaction in polymer electrolyte membrane fuel cell, Electrochim. Acta, 119 (2014) 144-154. https://doi.org/https://doi.org/10.1016/j.electacta.2013.12.072

Credit Author Statement
Peiqi Du: Experiments.
Jinwen Shi: Writing.
Jing Zhan: Experiment-surface area measurements with CO stripping method.
Lei Fu: Experiment-AFM and data processing.

Fei Liu: Data analysis, writing.

Declaration of interests

☒ The authors declare that they have no known competing financial interests or personal relationships that could have appeared to influence the work reported in this paper.

☐ The authors declare the following financial interests/personal relationships which may be considered as potential competing interests: